J Mater Sci (2008) 43:1525–1531
DOI 10.1007/s10853-007-2361-8

The effect of the cerium precursor and the carbon surface chemistry on the dispersion of ceria on activated carbon

Enrique V. Ramos-Fernández · Juan C. Serrano-Ruiz · Joaquín Silvestre-Albero · Antonio Sepúlveda-Escribano · Francisco Rodríguez-Reinoso

Received: 3 October 2007 / Accepted: 28 November 2007 / Published online: 1 January 2008

Abstract Activated carbon-supported cerium dioxide (CeO_2/C) was prepared by impregnation of a commercial support (Norit R2030) with aqueous solutions of two different cerium precursors, $[(NH_4)_2Ce(NO_3)_6]$ and $Ce(NO_3)_3 \cdot 6H_2O$. The effect of carbon surface chemistry on the dispersion of ceria was studied by using two different carbon supports, the R2030 and the same material after an oxidation treatment with H_2O_2. Thus, four samples were obtained by combining the precursors and the supports. The prepared materials were characterized by thermogravimetry, nitrogen adsorption isotherms (77 K), X-ray diffraction, temperature-programmed desorption, temperature-programmed reduction and transmission electron microscopy, in order to study the degree of ceria dispersion over the supports. It was found that the best results in terms of ceria dispersion were obtained for the material prepared with the oxidized carbon and ammonium cerium nitrate as cerium precursor.

Introduction

Cerium dioxide has a crucial role in a large number of important catalytic reactions and represents the most significant among the oxides of rare earth elements in industrial catalysis [1]. Ceria is especially relevant in two of the more important commercial catalytic processes: three-way catalysts (TWC) and fluid catalytic cracking (FCC). Furthermore, CeO_2 is used as promoter in several other reactions such as CO oxidation [2], catalytic wet oxidation [3], selective hydrogenation of unsaturated aldehydes [4–6] and *iso*-butane dehydrogenation [7]. However, cerium oxide presents several drawbacks which partially limit all the aforementioned catalytic applications of this material. First, it is very difficult to synthesize it with high surface area, typical values ranging from 50 to 150 $m^2\ g^{-1}$. The second important limitation of cerium dioxide is related to its textural stability under high temperature reaction conditions. Thus, a thermal treatment at 1,000–1,100 K can induce the growth of the CeO_2 crystallites, with the subsequent loss of surface area until the level of a few square meters per gram [8]. Finally, another factor which discourages the use of pure ceria as support in catalysis is its cost, higher than that of more common supports like Al_2O_3, SiO_2, or carbon. All these reasons have therefore directed research toward finding new catalyst formulations with improved thermal stability and surface area of cerium dioxide. In this way, the mixing of ceria with other elements (especially Zr) in form of mixed oxides [9, 10] and the spreading of CeO_2 over a thermally stable support such as Al_2O_3 [11] have been revealed as optimal solutions. In this last case, the dispersion of ceria over a high surface area support produces, furthermore, a higher effectiveness in the metal–ceria interaction [6].

Carbon has a number of properties (inertness, thermal stability, high surface area and tunable surface chemistry) making this material a promising alternative to be used as support for cerium dioxide. Thus, CeO_2/C has been successfully applied as support of noble metal catalysts in a number of important processes. Selective hydrogenation of unsaturated aldehydes [6, 12], electrooxidation of alcohols involved in the fuel cell technology [13, 14] and catalytic

E. V. Ramos-Fernández · J. C. Serrano-Ruiz · J. Silvestre-Albero · A. Sepúlveda-Escribano (✉) · F. Rodríguez-Reinoso
Departamento de Química Inorgánica, Universidad de Alicante, Apartado 99, 03080 Alicante, Spain
e-mail: asepul@ua.es

wet oxidation of pollutants in wastewater [15] are some of the examples that can be found in the literature. However, the study of the factors determining the degree of ceria dispersion on the carbon support has not received a detailed attention. The objective of this work is to investigate on two of these factors: the cerium dioxide precursor and the surface chemistry of the carbon support. To fulfill this goal two different cerium salts and one commercial carbon with different oxidation treatments were utilized to prepare four different samples. These samples were characterized by a number of techniques involving thermogravimetry (TG), nitrogen adsorption at 77 K, X-ray diffraction (XRD), temperature-programmed desorption (TPD), temperature-programmed reduction (TPR) and transmission electron microscopy (TEM) in order to evaluate the degree of ceria dispersion on the carbonaceous support.

Experimental

A commercial activated carbon supplied by Norit (R2030 CO_2), with 0.5–1.0 mm particle size, was used as initial support and labeled as "C". This carbon was treated with a 6 M solution of H_2O_2 (Scharlau, 35%) for 24 h. Then, it was washed with ultrapure water (until no oxidant character was detected using an acid aqueous solution of $KMnO_4$), dried at 373 K for 12 h and referred as "C_{ox}". Each carbon sample was impregnated with aqueous solutions of two different cerium salts: a Ce(IV) precursor $(NH_4)_2Ce(NO_3)_6$ and a Ce(III) precursor $Ce(NO_3)_3{\cdot}6H_2O$, with the adequate concentration to obtain a nominal CeO_2 loading of 20 wt.%. The actual loading was determined by repetitive calcinations and weighting; in all cases, it was 20 ± 0.5 wt.%. The excess of solvent was removed by gentle heating and finally they were dried at 373 K overnight. Four different samples were thus obtained: Ce(III)/C, Ce(IV)/C, Ce(III)/C_{ox} and Ce(IV)/C_{ox}. The decomposition of the cerium precursor to obtain CeO_2/C was accomplished under flowing helium (50 mL min^{-1}) at 523 K for 4 h, with a heating rate of 5 K min^{-1}.

The thermal decomposition of activated carbon-supported ceria precursors in an inert atmosphere was investigated by means of thermogravimetric experiments coupled to mass spectrometry (TG-MS). The weight loss during the heat treatment of the fresh impregnated carbon was analyzed with a SDT 2960 Simultaneous DSC-TGA. The measurement was carried out under helium atmosphere (100 mL min^{-1}), with a heating rate of 10 K min^{-1}. The gaseous products evolved were analyzed by mass spectrometry, following the evolution of signals corresponding to CO, CO_2, NO, N_2O and H_2O.

The textural properties of the prepared materials were determined by nitrogen adsorption at 77 K with a Coulter Omnisorp 610 system. Before measurements, the samples were dried at 383 K for 12 h and out-gassed at 523 K under vacuum. The micropore volume, V_{micro}, was calculated by application of the Dubinin–Radushkevich (DR) equation. The volume of mesopores, V_{meso}, was estimated by subtracting the volume of micropores from the total uptake at a relative pressure of 0.99. Surface area was calculated following the BET method.

X-ray powder diffraction patterns were recorded on a JSO Debye-flex 2002 system, from Seifert, fitted with a Cu cathode an a Ni filter, using a 2 min^{-1} scanning rate.

Temperature-programmed experiments were carried out in a U-shaped quartz cell using a He gas flow of 50 cm^3 min^{-1} (5% H_2/He in the case of TPR) and about 100 mg of sample, with a heating rate of 10 K min^{-1}. The reactor inlet and outlet gases were analyzed by mass spectrometry.

Conventional TEM was carried out with a JEOL model JEM-2010 electron microscope working at 200 kV and equipped with an INCA Energy TEM100 analytical system and a SIS MegaView II camera. Samples for analysis were suspended in methanol and placed on copper grids with a holey-carbon film support.

Results and discussion

Thermogravimetry

The thermal decomposition of the carbon-supported ceria precursors, Ce(IV)/C and Ce(III)/C, in an inert atmosphere was monitored by TG (Fig. 1). Several ranges with different slopes can be observed in both samples. The first weight loss stage, from room temperature up to 403 K, can be ascribed to the evolution of adsorbed water. The sharpest weight loss takes place from 423 to 483 K in both cases, and corresponds to the evolution of mainly NO, as deduced from mass spectrometry analysis, which is produced by the decomposition of the cerium nitrate precursors. Small amounts of N_2O are also produced in this step, although the main N_2O evolution is observed between 483 and 573 K. Above 573 K, there is still a slow weight loss that continues up to 773 K, which is related to the gasification of the carbon support with evolution of carbon monoxide, as a result of the reaction with nitrogen oxides remaining on the carbon surface [16]. It is remarkable that the total weight loss due to precursors decomposition is appreciably higher in the case of Ce(IV)/C (Fig. 1b) as it is expected in views of the molecular formula of the cerium precursors. With regard to samples supported on the oxidized carbon, C_{ox}, the same decomposition profiles were found and no appreciable differences with their respective non-oxidized counterparts could be observed. Thus, the decomposition of the cerium precursors finishes in all cases

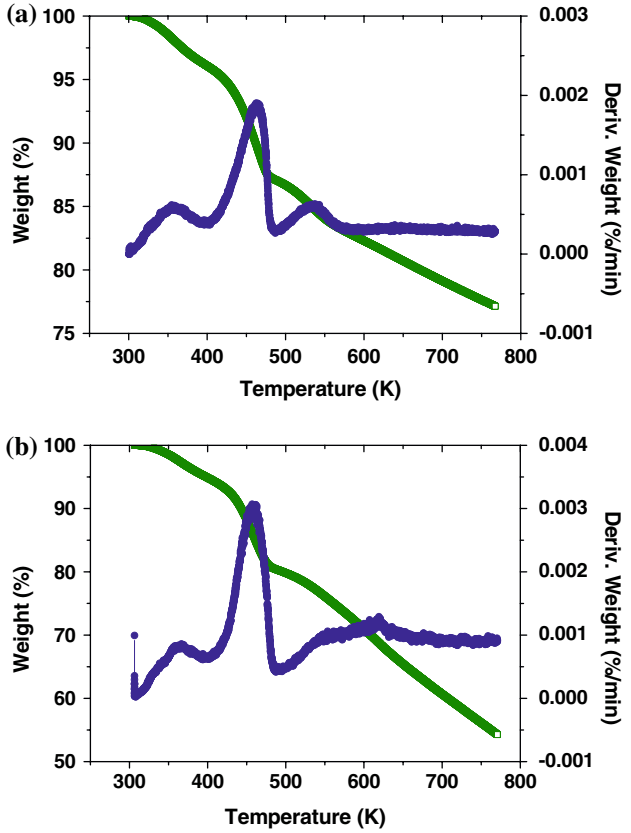

Fig. 1 TG profiles of the fresh impregnated carbon supports under helium: (**a**) Ce(III)/C and (**b**) Ce(IV)/C

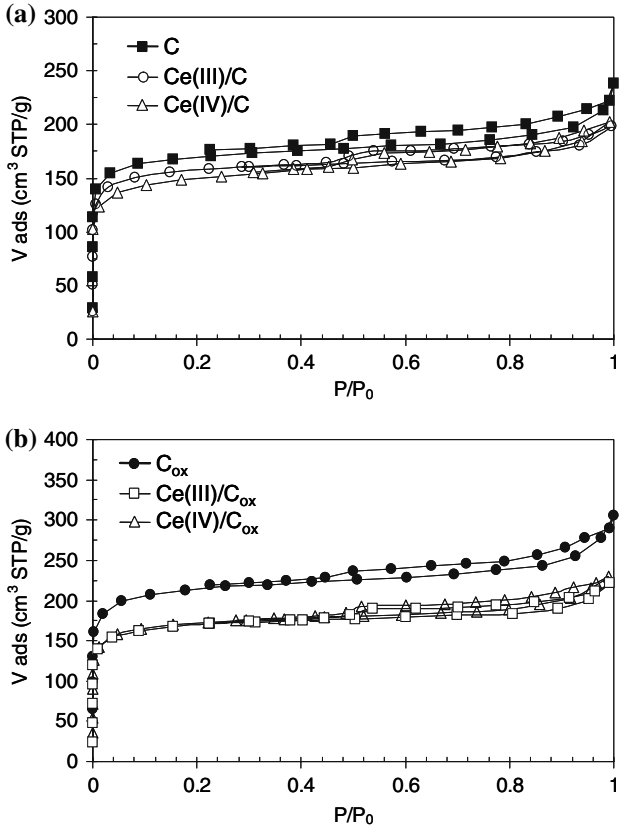

Fig. 2 N_2 adsorption isotherms at 77 K for: (**a**) samples supported on unoxidized carbon C and (**b**) samples supported on oxidized carbon C_{ox}

at about 573 K, and this was the selected temperature for the mentioned process.

N_2 adsorption isotherms

Figure 2 includes the adsorption isotherms of N_2 at 77 K for the carbon supports (C and C_{ox}), as well as for CeO_2/C and CeO_2/C_{ox} samples (after a decomposition treatment at 573 K for 4 h). A type I isotherm was observed in all cases, in which adsorption and desorption branches are not coincident (hysteresis loop), thus indicating the presence of a certain volume of mesopores (see Table 1). However, the analysis and the shape of the adsorption isotherms indicate that the porosity is, in all cases, basically constituted by micropores. It can be observed in Table 1 that the oxidation treatment produced an increase in the N_2 adsorption capacity (V_{micro} increases from 0.27 to 0.34 $cm^3\ g^{-1}$ and BET area from 654 to 820 $m^2\ g^{-1}$). This is caused by a slight gasification of the carbon due to the decomposition of oxygen surface groups introduced by oxidation upon the out-gassing process prior to the adsorption run, as the oxidation treatment is too weak to produce an activation of the carbon by itself. The adsorption capacity diminishes after CeO_2 deposition [17]. This decrease is small in the case of the parent C support (Fig. 2a), but more important for the oxidized carbon C_{ox} (Fig. 2b). Thus, a part of the micropores in C_{ox} was blocked by CeO_2 (V_{micro} decreases from 0.34 to 0.26 $cm^3\ g^{-1}$), and this is accompanied by a decrease in BET surface area (from 820 to 650 $m^2\ g^{-1}$). This could indicate that in the case of oxidized support the ceria particles are able to be located in the most internal part of the pores, blocking the narrowest microporosity. Thus, it can be deduced from these results that the oxidation treatment could have a beneficial effect on the dispersion of ceria over the carbon support.

Table 1 Textural properties of the carbon supports and CeO_2/C

Sample	V_{micro} ($cm^3\ g^{-1}$)	V_{meso} ($cm^3\ g^{-1}$)	S_{BET} ($m^2\ g^{-1}$)
C	0.27	0.10	654
Ce(III)/C	0.25	0.06	605
Ce(IV)/C	0.24	0.07	565
C_{ox}	0.34	0.13	820
Ce(III)/C_{ox}	0.27	0.07	651
Ce(IV)/C_{ox}	0.26	0.10	657

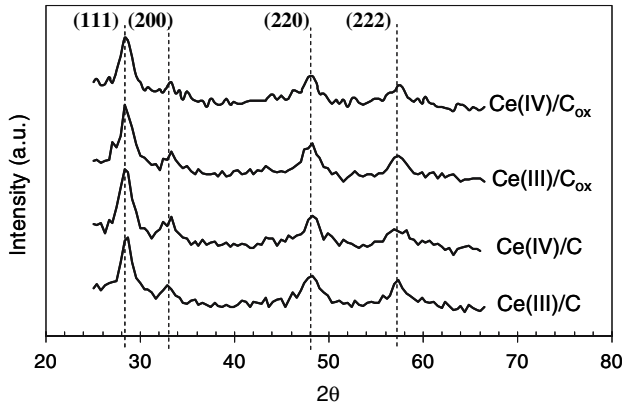

Fig. 3 XRD patterns for CeO_2/C samples

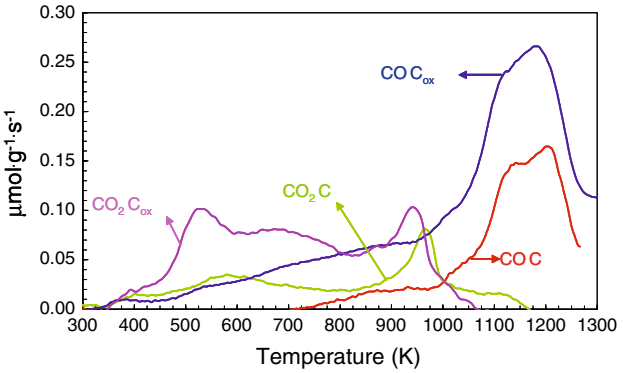

Fig. 4 TPD spectra (evolution of CO and CO_2) of the C and C_{ox} activated carbons

XRD patterns

The XRD patterns for the CeO_2/C samples, after the treatment in helium at 573 K are reported in Fig. 3. Four peaks (vertical lines) at 2θ values of 28.6, 33.4, 47.8 and 56.7 were detected in all cases. These peaks are produced, respectively, by the reflections of the (111), (200), (220) and (222) crystallographic planes of the cubic CeO_2 phase (JCPDS file 34-0394). A small CeO_2 particle size and, thus, a high degree of ceria dispersion over the carbon supports can be deduced from the broad diffraction peaks. The determination of the CeO_2 crystal sizes was carried out using the Scherrer equation, on the basis of the full width at half maximum (FWHM) of the (111) diffraction peak at $2\theta = 28.6°$, and the results are reported in Table 2. It can be seen that ceria crystallite sizes range from 6.6 to 5.8 nm, in good agreement with those calculated by Serrano-Ruiz et al. [12] for Pt–Sn/CeO_2/C catalysts (5.4 nm). However, these values are notably lower than those reported for unsupported crystalline CeO_2 (22.3 nm) [11]. If the different samples studied here are compared, the one prepared with the Ce(IV) precursor and the oxidized carbon as support, Ce(IV)/C_{ox}, showed the lower values of ceria crystal size (5.8 nm), which is in agreement with the results reported above, in the previous section.

Table 2 CeO_2 particle size for CeO_2/C samples and unsupported crystalline CeO_2[a]

Sample	CeO_2 particle size (nm)
Ce(III)/C	6.6
Ce(IV)/C	6.4
Ce(III)/C_{ox}	6.3
Ce(IV)/C_{ox}	5.8
Massive CeO_2	22.3

[a] Data obtained from Ref. [18]

Temperature-programmed desorption

The surface oxygen groups on both carbon supports, C and C_{ox}, were characterized by means of TPD. It is well known that these surface functionalities decompose upon heating in an inert atmosphere, evolving CO and CO_2 at different temperatures [18]. Figure 4 shows the evolution of CO and CO_2 as a function of temperature. As it can be clearly seen, the parent carbon C contains surface oxygen groups that decompose evolving mainly CO at high temperatures. Figure 4 also shows that carbon C exhibits two well-defined CO_2 desorption peaks, centered at about 588 and 973 K. The first desorption peak at low temperature corresponds to the decomposition of the less stable carboxylic acid groups, while the high temperature peak can be assigned to the decomposition of lactones-like groups [19, 20]. The TPD profile of carbon C_{ox} also showed one low temperature CO_2 desorption peak centered at about 538 K (with a very prominent shoulder at 693 K) and one at higher temperature (950 K) peak, which can be attributed, in the same way as for the C carbon, to the decomposition of carboxylic acid and lactone groups, respectively. However, the amount of these surface groups in the oxidized sample is higher, since more intense peaks were detected. With regard to the CO evolution, the TPD profile of carbon C showed one peak at 1,213 K with an intense shoulder at lower temperature (1,149 K), which can be originated by the decomposition of phenol, ether and carbonyl/quinone surface groups [6]. A more intense CO desorption peak, centered at 1,193 K, was observed for the oxidized sample, this indicating a higher amount of surface functionalities, as expected.

Temperature-programmed reduction

Figure 5 shows the evolution of the H_2 consumption as a function of temperature for the four CeO_2/C samples

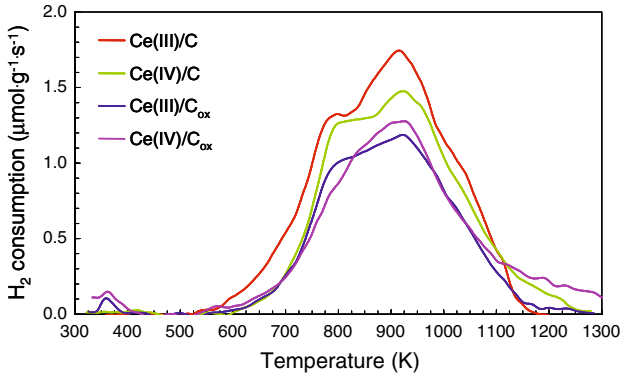

Fig. 5 TPR profiles of the CeO_2/C samples

studied. The TPR profiles include, in all cases, one broad reduction peak with a maximum centered at around 930 K. These profiles are quite different from those obtained for unsupported CeO_2. The typical reduction profile for massive CeO_2 consists of two reduction peaks, a smaller one at low temperature (773–823 K) and the second one, much more intense, at higher temperatures (1,163–1,173 K), which are associated to the reduction of surface and bulk ceria, respectively [21, 22]. Furthermore, a correlation has been observed between the ratio of the area of both reduction peaks and the surface area of the CeO_2 sample. In this way, the area below the low temperature reduction peak is relatively larger for high surface area CeO_2 [23]. Figure 5 shows that, in our case, only one continuous reduction process was observed, which is produced at lower temperatures (930 K) than the bulk ceria reduction (1,173 K). This could be indicative, as discussed above, of a high dispersion of cerium oxide on the carbon supports, with a very small CeO_2 particle size; this would lead to an easier reduction of ceria phase with respect to the unsupported oxide. When the reduction profiles of the different samples studied are compared, it can be observed that three of the samples, those supported on the as-received carbon, Ce(III)/C and Ce(IV)/C, and Ce(III)/C_{ox}, show a prominent shoulder at 803 K. This shoulder at lower temperatures has been previously attributed to the reduction of surface ceria whereas the rest of the reduction peak is assigned to reduction of bulk CeO_2 [7]. The sample prepared with the Ce(IV) precursor supported on oxidized carbon did not present the mentioned shoulder, this indicating that the ceria particle size in these samples is very small and no distinction can be made between surface and bulk ceria. Consequently, surface chemistry of carbon seems to play an important role in the ceria dispersion process, as will be seen in the next section.

Transmission electron microscopy

Figure 6 shows the TEM images for the four CeO_2/C samples. Dark zones are due to cerium oxide whereas

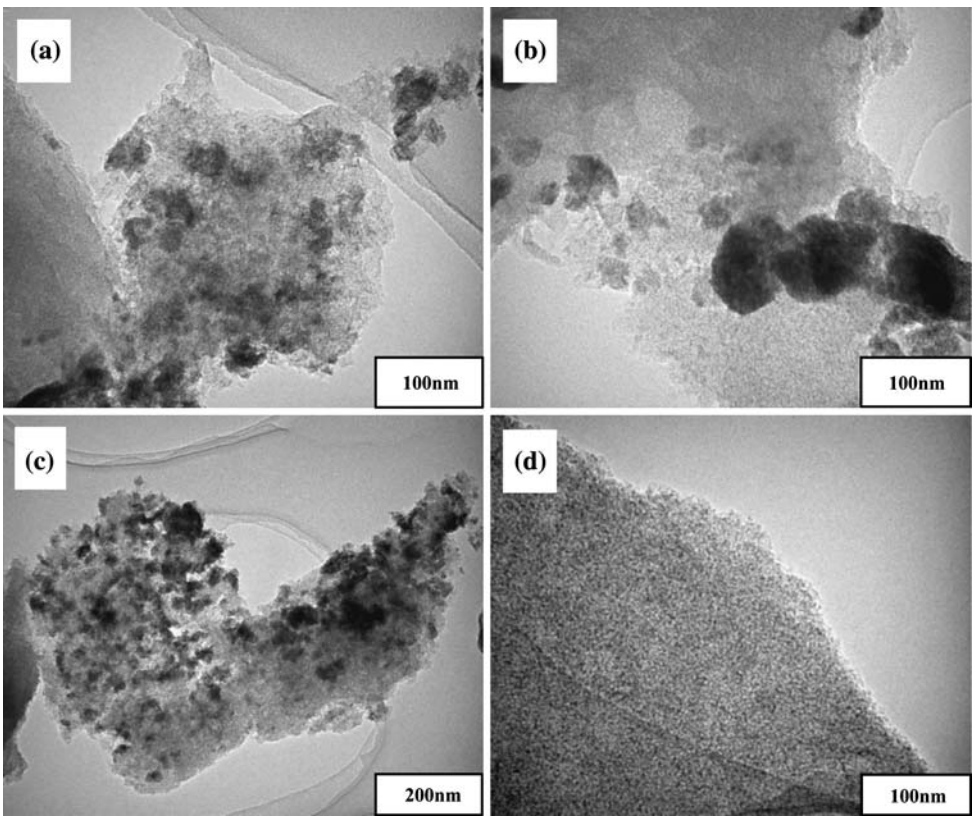

Fig. 6 TEM micrographs of CeO_2/C samples: (**a**) Ce(III)/C; (**b**) Ce(IV)/C; (**c**) Ce(III)/C_{ox} and (**d**) Ce(IV)/C_{ox}

lighter parts correspond to carbon. From the analysis of the images it can be concluded that in all samples, except in Ce(IV)/C_{ox}, there is a certain degree of agglomeration of the ceria particles over the carbon surface. However, the images corresponding to Ce(IV)/C_{ox} gave evidence of a more homogeneous distribution of ceria, with a very low number of agglomerations. These results are in good agreement with those obtained by XRD (see Table 2) and TPR (Fig. 5). A tentative explanation for these findings can be proposed, taking into account the specific characteristics of both the ceria precursors and the carbon surface chemistry (Fig. 7). The Ce(IV) precursor, $(NH_4)_2Ce(NO_3)_6$, forms an anionic cerium complex in aqueous solution. This complex can interact with the oxidized carbon support in two ways: (i) it can interact with the acid surface oxygen groups of the carbon support to produce nitric acid via the NO_3^- ligands, and (ii) it can be electrostatically adsorbed on the carbon support, since the aqueous solution of this complex has a pH of 0.5, well below the point of zero charge of the carbon surface. Under these circumstances the carbon surface has a strong affinity to interact with anions. The oxidation treatment to obtain C_{ox} is not very strong and thus the point of zero charge of carbon is hardly decreased. However, it does generate enough acid groups (see Fig. 4) to establish an interaction with the complex via the nitrate ligands. It must be mentioned that some other tests were carried out with a strongly oxidized carbon (treated with HNO_3) and ceria dispersion was not improved. In this case the more drastic oxidation treatment produced a strong decrease of the point of zero charge of carbon, this inducing a lower electrostatic interaction between the ceria precursor and the carbon surface and finally, a poorer dispersion. Thus, the combination of a mild oxidation treatment and a cerium (IV) precursor produces a high carbon surface–ligand interaction based in an optimal difference between the pH of the precursor solution and the point of zero charge of the carbon surface.

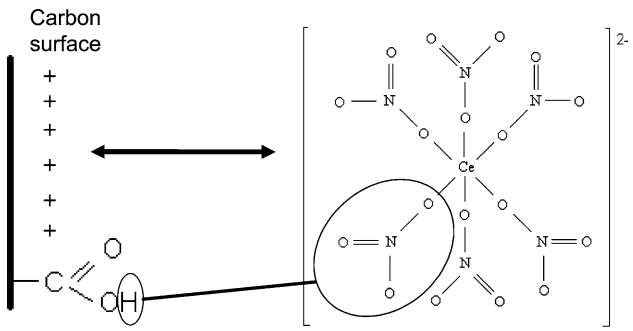

Fig. 7 Proposed scheme for the interaction between oxidized carbon surface and Ce(IV) precursor in solution

Conclusions

This work reports the influence of the cerium precursor and the surface chemistry of carbon on the ceria dispersion in CeO_2/C materials. Thus, four different CeO_2/C samples were prepared by an impregnation method and by combining two different cerium precursors, $[(NH_4)_2Ce(NO_3)_6]$ and $Ce(NO_3)_3{\cdot}6H_2O$, and two carbon supports with different degree of surface oxidation, C and C_{ox}. After a treatment in helium at 573 K the total decomposition of cerium precursors was achieved with the formation of a cubic CeO_2 phase dispersed on carbon. XRD, TPR and TEM experiments showed that the combination of a Ce(IV) precursor and a slightly oxidized carbon support leads to an optimal ceria dispersion.

Acknowledgements Financial support from the Ministerio de Educación y Ciencia (Spain), Projects BQU 2003-06150 and MAT2004-03480-C02-02, and the Network of Excellence InsidePores, European Commission Contract No. NMP3-CT2004-500895, is gratefully acknowledged.

References

1. Trovarelli A, De Leitenburg C, Boaro M, Dolcetti G (1999) Catal Today 50:353
2. Ayastuy JL, Gil-Rodríguez A, González-Marcos MP, Gutiérrez-Ortiz MA (2006) Int J Hydrogen Energy 31:2231
3. Delgado JJ, Pérez-Omil JA, Rodríguez-Izquierdo JM, Cauqui MA (2006) Catal Commun 7:639
4. Serrano-Ruiz JC, Luettich J, Sepúlveda-Escribano A, Rodríguez-Reinoso F (2006) J Catal 241:45
5. Sepúlveda-Escribano A, Coloma F, Rodríguez-Reinoso F (1998) J Catal 178:649
6. Sepúlveda-Escribano A, Silvestre-Albero J, Coloma F, Rodríguez-Reinoso F (2000) Stud Surf Sci Catal 130:1013
7. Serrano-Ruiz JC, Sepúlveda-Escribano A, Rodríguez-Reinoso F (2007) J Catal 246:158
8. Perrichon V, Laachir A, Abouarnadasse S, Touret O, Blanchard G (1996) Appl Catal A 129:69
9. Ozawa M, Kimura M, Isogai A (1993) J Alloys Compd 193:73
10. Ranga R, Kaspar J, Di Monte R, Meriani S, Graziani M (1994) Catal Lett 24:107
11. Mekhemer Gamal AH, Ismail Hamdy M (2004) Colloids Surf A Physicochem Eng Asp 235:129
12. Serrano-Ruiz JC, Sepúlveda-Escribano A, Rodríguez-Reinoso F, Duprez D (2007) J Mol Catal A 268:227
13. Xu C, Shen P (2004) Chem Commun 10:2238
14. Xu C, Zeng R, Kang Shen P, Wei Z (2005) Electrochim Acta 51:1031
15. Oliviero L, Barbier J Jr, Duprez D, Guerrero-Ruiz A, Bachiller-Baeza B, Rodríguez-Ramos I (2000) Appl Catal B 25:239
16. Ramos-Fernández EV, Serrano-Ruiz JC, Silvestre-Albero J, Sepúlveda-Escribano A, Rodríguez-Reinoso F, DOI: 10.1016/j.materresbull.2007.07.001
17. Rodríguez-Reinoso F, Martín-Martínez JM, Prado-Burguete C, Mcenaney B (1987) J Phys Chem 91:515
18. Rodríguez-Reinoso F, Molina-Sabio M (1998) Adv Colloid Interface Sci 76–77:271
19. Figueiredo JL, Pereira MFR, Freitas MMA, Orfao JJM (1999) Carbon 37:1379

20. Ríos RVRA, Silvestre-Albero J, Sepúlveda-Escribano A, Rodríguez-Reinoso F (2007) Colloids Surf A Physicochem Eng Asp 300:180
21. Fally F, Perrichon V, Vidal H, Kaspar J, Blanco G, Pintado JM, Bernal S, Colon G, Daturi M, Lavalley JC (2000) Catal Today 59:273
22. Aneggi E, Boaro M, De Leitenburg C, Dolcetti G, Trovarelli A (2006) J Alloys Compd 408–412:1096
23. Giordano F, Trovarelli A, De Leitenburg C, Giona M (2000) J Catal 193:273